Electronic Supplementary Material (ESI) for Analyst.

Supporting Information

Impact of physical and chemical parameters on square wave anodic stripping voltammetry for trace Pb^{2+} analysis in simulated water

Connor E Rahm, Pankaj Gupta, Vandna K. Gupta, Artur Huseinov, Ben Griesmer, and *Noe T. Alvarez

Department of Chemistry, University of Cincinnati, Cincinnati, OH 45221, United States

*Email: alvarene@ucmail.uc.edu

Table S1. Real water sample measured parameters.

pH	Conductivity ($\mu S\ cm^{-1}$)	Free Chlorine ($mg\ L^{-1}\ Cl_2$)	$CaCO_3$ ($mg\ L^{-1}$)	Copper ($\mu g\ L^{-1}$)	Lead ($\mu g\ L^{-1}$)
9.0 ± 0.1	363 ± 4	0.45 ± 0.03	133 ± 5	0.22 ± 0.02	0.03 ± 0.03

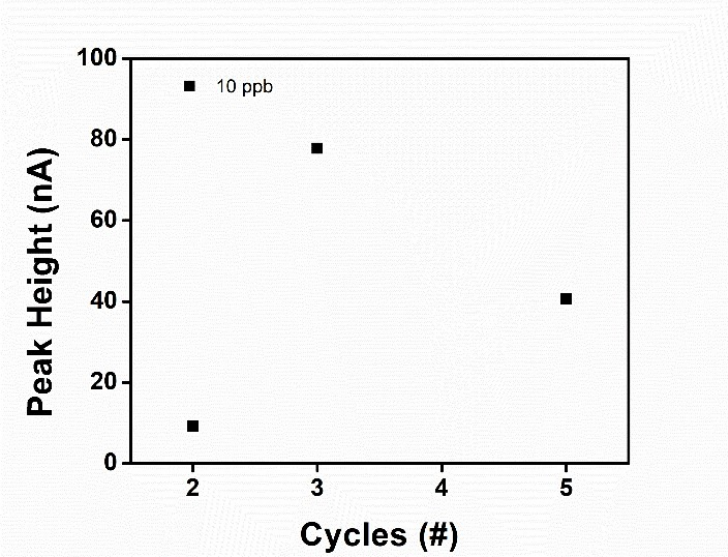

Fig. S1 SWASV determinations of 10 ppb Pb^{2+} in 0.1 M aceate buffer (pH = 4.3) at the AuNP-CNT*f*-CS electrodes modified with 2, 3, or 5 CV cycles during gold electrodeposition.

Raman spectroscopy:

Experiment details: Raman spectroscopy were carried out using a Renishaw inVia Raman microscope, excited by a 633 nm Ar-ion laser, Gloucestershire UK. Raman spectra were collected at 5 points for each CNT*f* cross section sample using ~ 30 s acquisition time with 10%

power. The time and power are kept constant during surface enhanced Raman spectroscopy (SERS) studies.

Raman spectroscopy is a very important and unique tool to characterize metal nanoparticle (NP) deposition on CNT surfaces. It is well known the effect of metal nanoparticle on the substrate give enhancement in Raman intensity due to localized surface plasmon resonance (LSPR) in visible light [1–3]. The enhancement factor (EF) depends on many paraments like shape, size, and density of NPs. Generally, Au [4,5], Ag [6] and Cu metal nanoparticles [7,8] are used for SERS substrates, where Au and Ag NPs give the highest SERS enhancement. Here, the Raman spectroscopy is performed on the AuNP-CNT*f*-CS electrode surface.

.

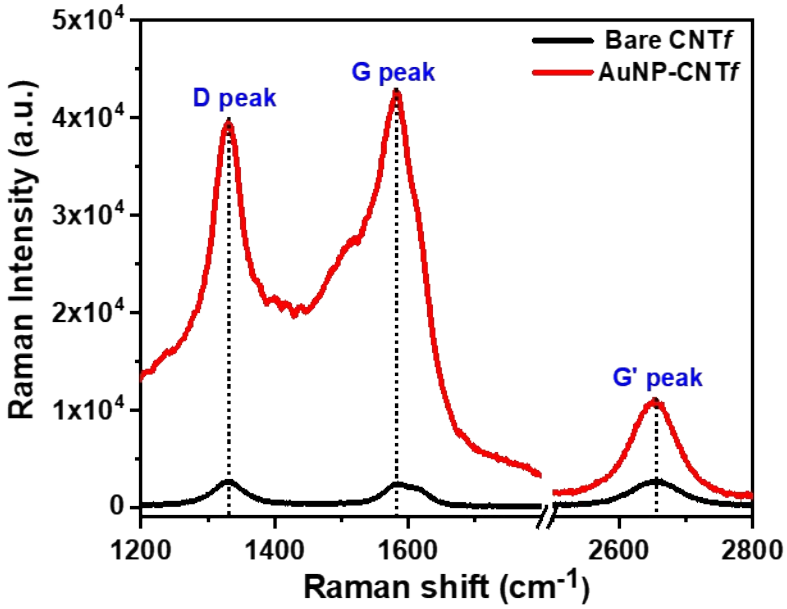

Fig. S2 Raman spectra of (black-bottom) bare CNT*f* cross-section and (red-top) AuNPs-CNT*f* cross-section. AuNPs were deposited using three cycle CV modification.

The representative Raman spectra of bare CNT*f*-CS (black) and AuNP-CNT*f*-CS (red) are shown in Fig. S2 wherein, mainly three Raman peaks for CNTs are observed as *D* peak (~1332 cm^{-1}), *G*

peak (~1582 cm^{-1}), G' peak (~2655 cm^{-1}) using 633 nm incident laser wavelength. For the bare CNT*f*-CS surface, the Raman relative intensities of the D peak are ~ 2700, while intensity of G and G' peak are observed ~ 2400 and 2500 counts. After modification with AuNPs, the EF for D, G and G' Raman peaks are observed ~ 14, 18 and 4, respectively. Sharma et al. [9] reported the EF ~ 5 for G peak on Au deposited MWCNTs side walls. When light interacts with matter, the enhancement in intensity is observed, due to the resonance that occurs between high electric fields generated by the incident radiation and the surface plasmons on Au-CNT substrate that result in Au nanoparticles to generate their own dipolar field and increase absorption in the nearby [9]. Our recently published paper [8] has shown the 3-times lower EF for D and G peaks on CuNP modified high density CNT*f*-CS surface.

Electrochemical impedance spectroscopy

Experimental details: Gamry Reference 600 potentiostat was used to record electrochemical impedance spectroscopy (EIS) data using a three-electrode cell consisting of HDCNT as the working electrode, a Ag|AgCl reference electrode, and a platinum wire counter electrode. The electrolyte used was 5 mM $K_3Fe(CN)_6$ and 0.1 M KCl as supporting electrolyte at 10 mV vs. Ag/AgCl in the frequency range 10^6 -1 Hz.

When metallic nanoparticles are deposited on the CNT surface, the performance of the CNT based electrode can be further improved due to an increased surface area. So, the electrochemical impedance spectroscopy (EIS) technique was used to characterize the physical and interfacial properties of the CNT*f*-CS and modified AuNP-CNT*f*-CS electrodes. Nyquist plot shown in Fig. S3 consists of two important features 1) semicircle (at high frequencies) and 2) the straight line at 45^0 known as a semi-infinite diffusion (at low frequencies). Spectra were fitted using Randles equivalent circuit. Charge transfer resistance (R_{ct}) values can be estimated from

the diameter of the semicircle feature at higher frequencies of the Nyquist plot to reflect the interfacial properties of electrodes. Here, the solution resistance (R_s) and R_{ct} are observed ca 247 Ω and 1316 Ω, respectively for bare surface however after modification with AuNPs, the R_s and R_{ct} values were decreased down to 198 Ω and 589 Ω, respectively as shown in Fig. S3. The reduction in R_{ct} can be attributed to the increase in geometrical surface area after AuNPs deposition.

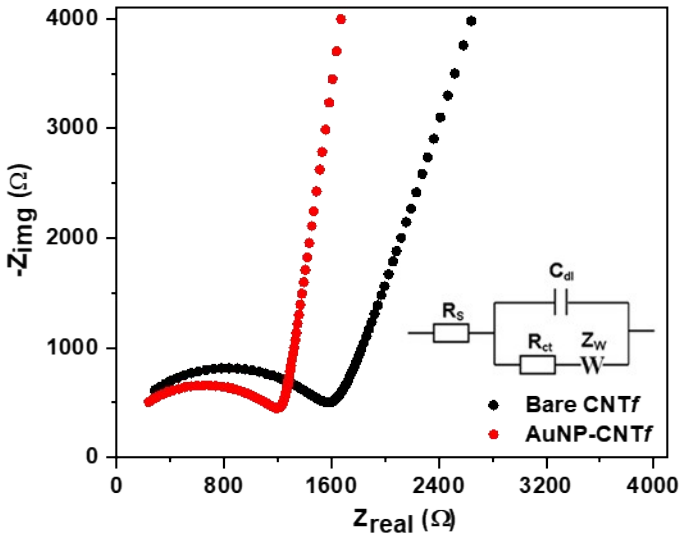

Fig. S3 Nyquist plots of (black-top) bare CNT*f*-CS and (red-bottom) AuNP-CNT*f*-CS micro electrodes (inset is Randles equivalent circuit).

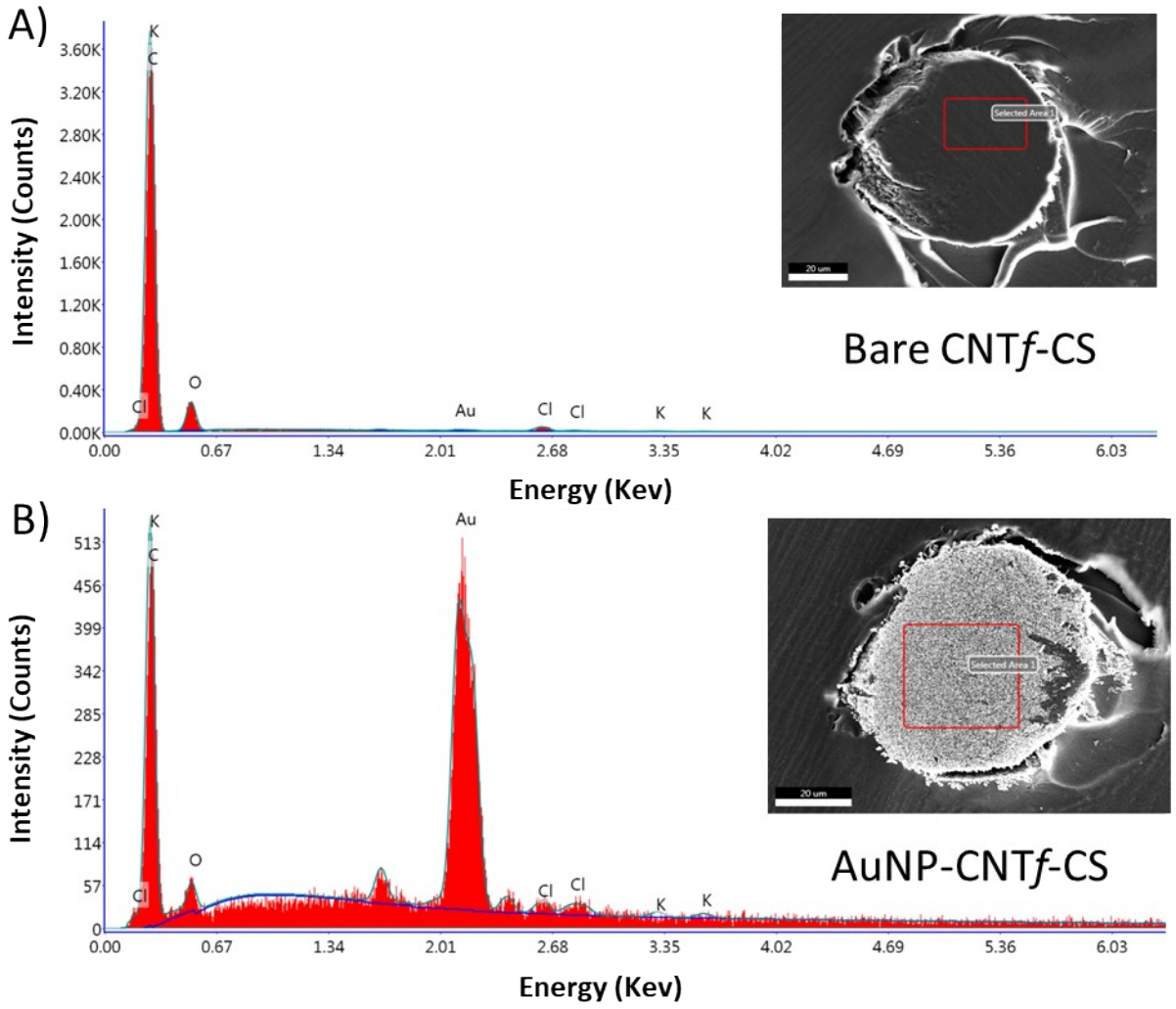

Fig. S4 Energy dispersive X-ray (EDAX) spectroscopy at (A) the bare CNT*f*-CS and (B) the AuNP-CNT*f*-CS electrodes. Insets are the SEM micrograms showing a red box around analyzed areas.

Energy dispersive X-ray (EDAX) spectroscopy was performed on an A FEI Apreo 2 C from Thermo Scientific microscope. EDAX spectra were collected with electron beam energy of 10 keV, 7 mm working distance, an acquisition time of 30 seconds, and a representative area of each electrode surface was analyzed.

Table. S2 TEAM™ eZAF EDS Smart Quant software results for the elemental analysis and weight % of the bare CNT*f*-CS, and AuNP-CNT*f*-CS samples

Element	**Weight % (Bare CNT*f*-CS)**	**Weight % (AuNP-CNT*f*-CS)**
Gold	**0.8**	**57.1**
Carbon	85.1	37.5
Oxygen	12.2	2.8
Chlorine	1.7	1.6
Potassium	0.3	1.0

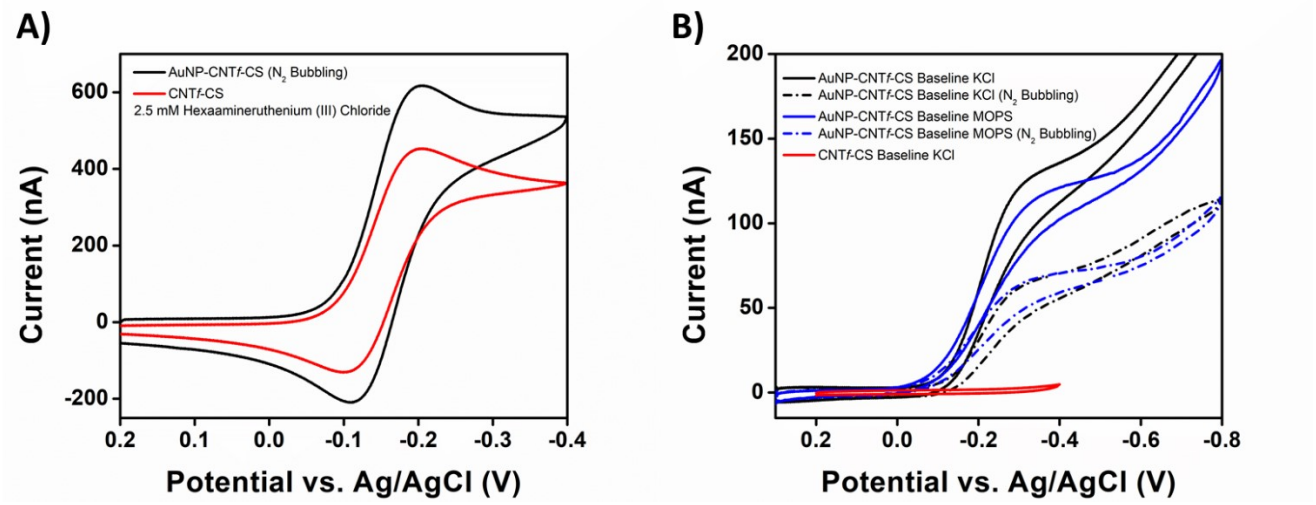

Fig. S5 Cyclic voltammograms (A) in 0.1 M KCl solution with 2.5 mM hexaaminеruthenium (III) chloride at the (black) AuNP-CNT*f*-CS and (red) bare CNT*f*-CS electrode surfaces, and (B) in (black) 0.1 M KCl and in (blue) 0.1 M MOPS standard solution at the AuNP-CNT*f*-CS electrode surface (dash-dot) with and (solid) without N_2 gas bubbling for 5-minutes prior, and (red) baseline of the bare CNT*f*-CS in 0.1 M KCl. 100 mV/s scan rate.

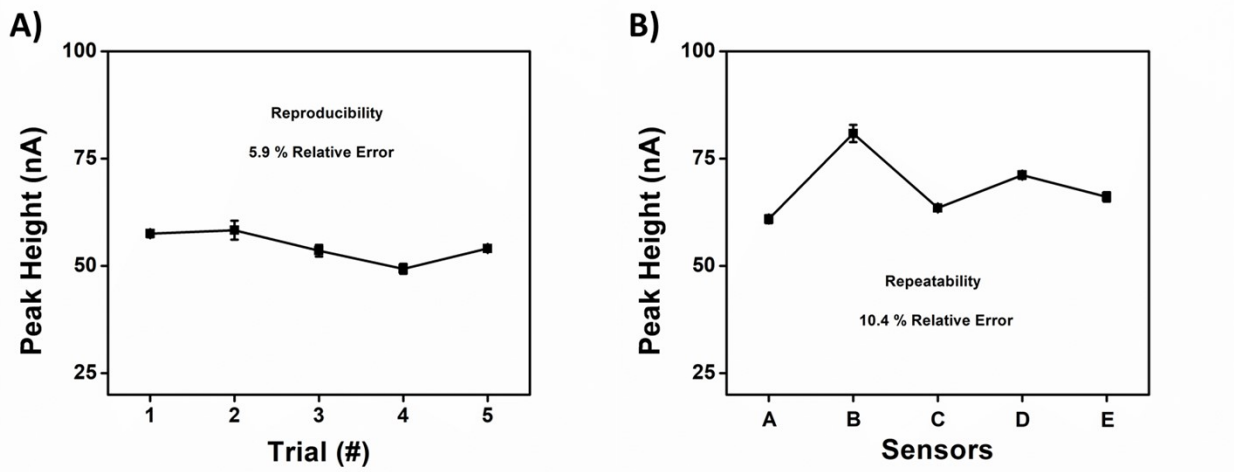

Fig. S6 Stability of the AuNP-CNT*f*-CS electrode. (A) Reproducibility of a single electrode during SWASV determinations in five separate simulated water samples with 10 ppb Pb^{2+} (n = 3), and (B) repeatability between five separate electrodes performing SWASV determinations of five separate simulated drinking water samples with 10 ppb Pb^{2+} (n = 3).

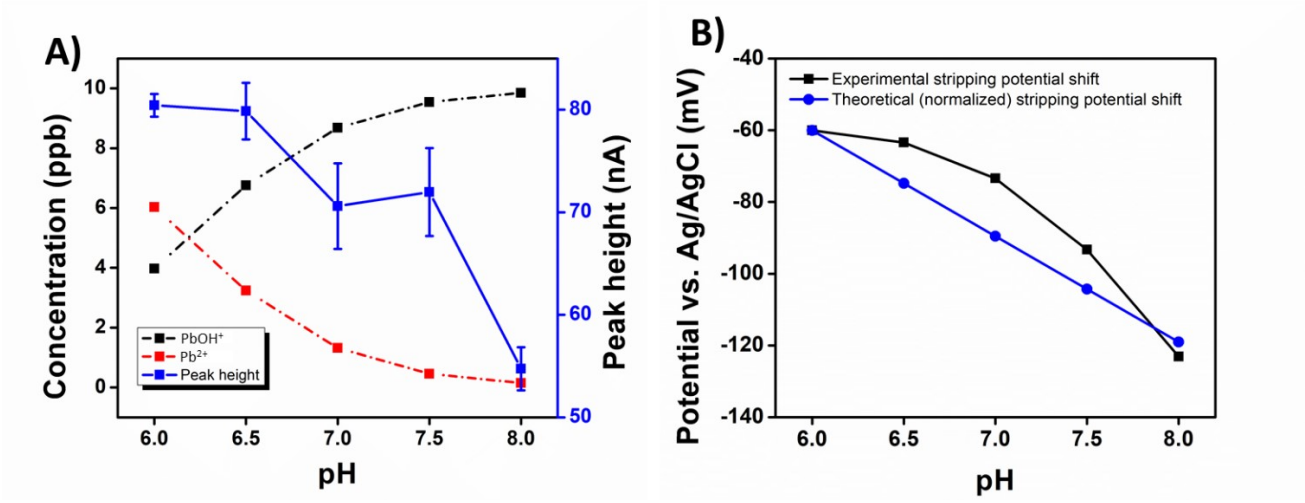

Fig. S7 (A) Theoretical equilibrium concentrations of Pb^{2+} and $PbOH^{+}$ with changing solution pH in 10 ppb Pb solution, plotted with the experimental peak height shifts of 10 µg L^{-} with pH. (B) Experimental and theoretical changes of reduction potential for $PbOH^{+}$ with pH.

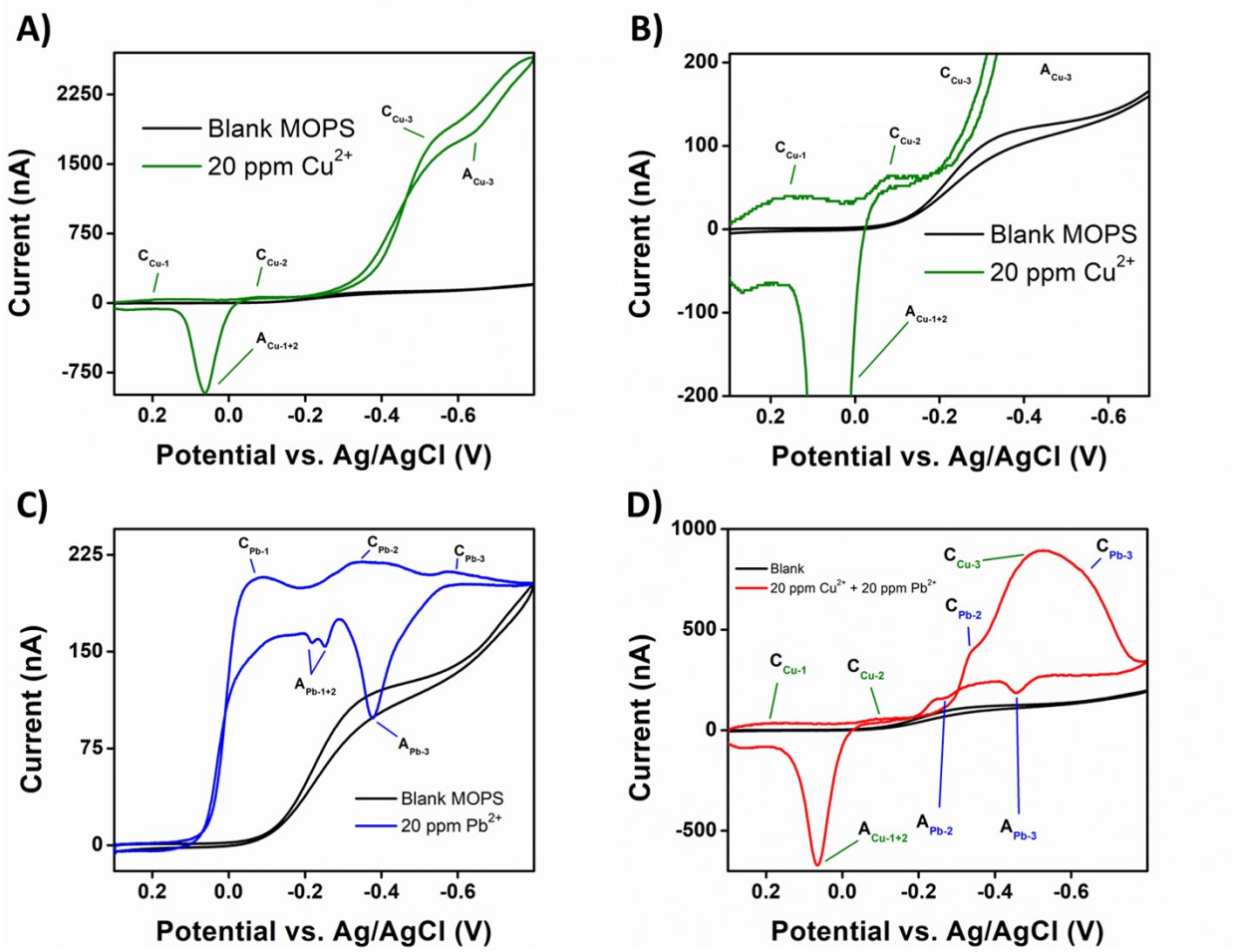

Fig. S8 Cyclic voltammograms in simulated water samples of MOPS buffer at pH = 7.0 and conductivity of 500 µS/cm, (A) 20 ppm Cu^{2+}, (B) 20 ppm Cu^{2+} with zoomed axis', (C) 20 ppm Pb^{2+}, and (D) 20 ppm of both Cu^{2+} and Pb^{2+} with all cathodic (C_x) and anodic (A_x) peaks annotated in each plot.

Fig. S7 shows the CV response of the Au-CNT*f* electrode in MOPS (pH = 7.0; conductivity 500 µS/cm) with the addition of 20 ppm Pb^{2+} and Cu^{2+} individually and simultaneously, with scan rate of 50 mV/s and potential window from +300 to -800 mV. Indicating that the electrochemical phenomenon underpotential deposition (UPD) occurs at the Au-CNT*f* electrode during Pb^{2+} reduction [10,11].

References

[1] U. Kreibig, M. Vollmer, Optical properties of metal clusters, Springer Berlin Heidelberg, Berlin, Heidelberg, 1995. doi:10.1007/978-3-662-09109-8.

[2] K.L. Kelly, E. Coronado, L.L. Zhao, G.C. Schatz, The optical properties of metal nanoparticles: The influence of size, shape, and dielectric environment, J. Phys. Chem. B. 107 (2003) 668–677. doi:10.1016/j.ocecoaman.2014.06.011.

[3] J.A. Creighton, D.G. Eadon, Ultraviolet-visible absorption spectra of the colloidal metallic elements, J. Chem. Soc. Faraday Trans. 87 (1991) 3881–3891. doi:10.1039/FT9918703881.

[4] X. Liang, N. Li, R. Zhang, P. Yin, C. Zhang, N. Yang, K. Liang, B. Kong, Carbon-based SERS biosensor: from substrate design to sensing and bioapplication, NPG Asia Mater. 13 (2021). doi:10.1038/s41427-020-00278-5.

[5] A.J. Caires, R.P. Vaz, C. Fantini, L.O. Ladeira, Highly sensitive and simple SERS substrate based on photochemically generated carbon nanotubes-gold nanorods hybrids, J. Colloid Interface Sci. 455 (2015) 78–82. doi:10.1016/j.jcis.2015.04.071.

[6] J.C. Valmalette, Z. Tan, H. Abe, S. Ohara, Raman scattering of linear chains of strongly coupled Ag nanoparticles on SWCNTs, Sci. Rep. 4 (2014) 1–8. doi:10.1038/srep05238.

[7] A. V. Markin, N.E. Markina, J. Popp, D. Cialla-May, Copper nanostructures for chemical analysis using surface-enhanced Raman spectroscopy, TrAC - Trends Anal. Chem. 108 (2018) 247–259. doi:10.1016/j.trac.2018.09.004.

[8] P. Gupta, V.K. Gupta, A. Huseinov, C.E. Rahm, K. Gazica, N.T. Alvarez, Highly sensitive non-enzymatic glucose sensor based on carbon nanotube microelectrode set, Sensors Actuators B Chem. 348 (2021) 130688. doi:10.1016/j.snb.2021.130688.

[9] H. Sharma, V. Kaushik, D. V. Avasthi, A.K. Shukla, V.D. Vankar, Au-nanoparticles-decorated MWCNTs demonstrating enhanced fluorescence and Raman spectroscopy, 58 (2012) 58–60. doi:10.1063/1.4732367.

[10] G. Herzog, D.W.M. Arrigan, Determination of trace metals by underpotential deposition-stripping voltammetry at solid electrodes, TrAC - Trends Anal. Chem. 24 (2005) 208–217. doi:10.1016/j.trac.2004.11.014.

[11] G. Martínez-Paredes, M.B. González-Garcaiaa, A. Costa-Garcia, Lead sensor using gold nanostructured screen-printed carbon electrodes as transducers, Electroanalysis. 21 (2009) 925–930. doi:10.1002/elan.200804496.